JOURNAL OF AIRCRAFT
Vol. 43, No. 6, November–December 2006

Effects of Tail Dihedral on Static Stability

W. F. Phillips,* A. B. Hansen,† and W. M. Nelson†
Utah State University, Logan, Utah 84322-4130

DOI: 10.2514/1.20683

It is shown that lifting-line theory closely captures the effects of tail dihedral on the static stability contributions of an aft tail and compares well with experiments. Such computations show that vortex interactions between the lifting surfaces of an aft tail can significantly affect tail performance. For a V-tail, these interactions slightly increase the tail's contribution to pitch stability and substantially decrease its contribution to yaw and roll stability. When horizontal-stabilizer dihedral is used in combination with a vertical stabilizer, it is shown that the tail will provide greater yaw stability if negative dihedral is used in horizontal stabilizers mounted below a vertical stabilizer. Conversely, positive dihedral works best in cases where the horizontal stabilizer is mounted above the vertical stabilizer.

Nomenclature

b = reference length
b_V = tip-to-tip V-tail span, measured normal to the plane of symmetry
b'_V = twice the V-tail root-to-tip semispan length, measured parallel with tail dihedral
C_L = lift coefficient
$C_{L,\alpha}$ = lift slope, change in lift coefficient with angle of attack
C_ℓ = rolling moment coefficient about the junction of the tail semispans
$C_{\ell,\beta}$ = roll-stability derivative, change in rolling moment coefficient with sideslip angle
$\tilde{C}_{L,\alpha}$ = airfoil section lift slope
$C_{L_i,\alpha}$ = local in situ section lift slope, including the effects of local induced downwash
C_Y = side-force coefficient
$C_{Y,\beta}$ = side-force derivative, change in side-force coefficient with sideslip angle
c = section chord length
L = vertical lift, positive upward
ℓ = rolling moment about the junction of the tail semispans, positive to the right
R_A = aspect ratio, b'^2_V/S'_V, not the horizontal projection
R_T = taper ratio
S = reference planform area
S'_V = twice the V-tail semispan planform area, measured parallel with tail dihedral
S_h = horizontal-stabilizer planform area
S_v = vertical-stabilizer planform area
V = airspeed
Y = side force, positive to the right
y = spanwise coordinate, measured normal to the plane of symmetry
y' = spanwise coordinate, measured parallel with stabilizer dihedral
α = reference line angle of attack
α_0 = semispan angle of attack at zero reference line angle of attack
α_{L0} = zero lift angle of attack
β = sideslip angle, positive for sideslip to the right (relative wind right to left)
Γ = dihedral angle, positive with tips above the root
κ_L = lift slope factor from lifting-line theory
κ_ℓ = planform factor for roll stability
κ_Γ = dihedral factor for roll stability
ρ = air density

Received 23 October 2005; revision received 7 December 2005; accepted for publication 7 December 2005.

*Professor, Mechanical and Aerospace Engineering Department, 4130 Old Main Hill. Member AIAA.
†Graduate Student, Mechanical and Aerospace Engineering Department, 4130 Old Main Hill. Student Member AIAA.

Introduction

TAIL dihedral, such as that shown in Fig. 1, can significantly influence the yaw stability derivative for an airplane [1]. With proper design in an aft tail, either positive dihedral (tips above the root) or negative dihedral (called anhedral) can increase the yaw stability of an airplane. If sufficient dihedral or anhedral is added to a conventional horizontal stabilizer, the vertical stabilizer can be eliminated completely to produce a V-tail, such as that shown in Fig. 2. The two semispans of this V-tail provide both pitch and yaw stability for the aircraft.

As a first approximation, the pitch and yaw stability derivatives for aft tail configurations such as those shown in Figs. 1 and 2 are sometimes estimated by simply computing the horizontal and vertical tail volume ratios using the horizontal and vertical projections of the total tail planform area, respectively. Such estimates should be used with caution, because they do not account for the aerodynamic interactions between the different lifting surfaces of the tail and these interactions can substantially alter tail performance.

The spanwise distribution of lift that is produced on a typical V-tail in pure sideslip is shown in Fig. 3. This lift distribution, which is the result of sideslip to the right with no aerodynamic angle of attack, has positive lift generated on the right semispan and negative lift on the left semispan. The vertical components of lift on the two semispans approximately cancel, producing little or no vertical force. Conversely, the horizontal components of lift on these two semispans combine to produce a net side force to the left that opposes the sideslip and is proportional to the sideslip angle.

When this same V-tail is operating at a positive angle of attack with no sideslip, it produces the lift distribution shown in Fig. 4. At this operating condition, the horizontal components of lift on the two semispans cancel and the vertical components combine to produce a net upward force that is proportional to the angle of attack. Thus, when this geometry is used as an aft tail, as shown in Fig. 2, it provides a stabilizing contribution to both the pitching and yawing moments for the complete aircraft. The magnitudes of the pitch and yaw stability derivatives can be controlled by adjusting the total area and dihedral angle.

An isolated V-tail operating at a positive angle of attack with no sideslip feels an upward component of relative wind equal to the airspeed multiplied by the sine of the angle of attack, $V \sin\alpha \cong V\alpha$.

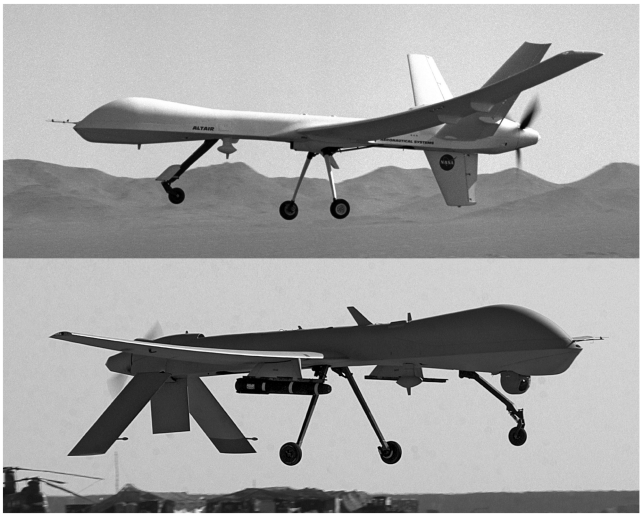

Fig. 1 Examples of tail dihedral shown in two tail configurations used on different models of the Predator UAV (NASA and U.S. Air Force photographs).

Fig. 2 Example of a V-tail used on the Global Hawk UAV (U.S. Air Force photograph).

Similarly, when the isolated V-tail is operating with positive sideslip and no angle of attack, it feels a leftward component of relative wind equal to the airspeed multiplied by the sine of the sideslip angle, $V \sin\beta \cong V\beta$. Thus, for small aerodynamic angles, the upward normal components of relative wind on the right and left semispans of a V-tail are closely approximated as

$$(V_{\text{normal}})_{\text{right}} \cong V\alpha\cos\Gamma + V\beta\sin\Gamma$$

$$(V_{\text{normal}})_{\text{left}} \cong V\alpha\cos\Gamma - V\beta\sin\Gamma$$

Accordingly, for small aerodynamic angles, the freestream angles of attack normal to the right and left semispans of a V-tail are closely approximated as [2]

$$\alpha_{\text{right}} \cong \frac{(V_{\text{normal}})_{\text{right}}}{V} \cong \alpha\cos\Gamma + \beta\sin\Gamma \tag{1}$$

$$\alpha_{\text{left}} \cong \frac{(V_{\text{normal}})_{\text{left}}}{V} \cong \alpha\cos\Gamma - \beta\sin\Gamma \tag{2}$$

Referring to Fig. 4, the vertical lift produced on each semispan of a V-tail is the lift produced normal to that semispan multiplied by $\cos\Gamma$. Similarly, the side force produced on the left semispan is the lift normal to that semispan multiplied by $\sin\Gamma$, and the side force on

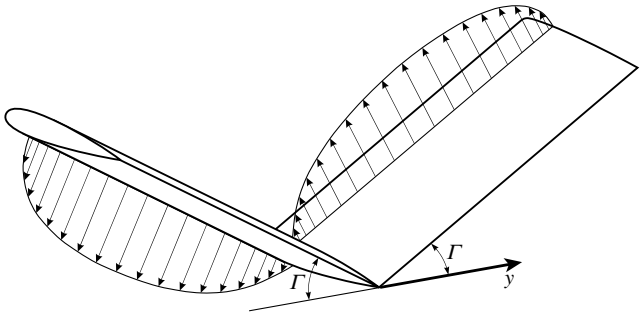

Fig. 3 Spanwise lift distribution on a V-tail in pure sideslip.

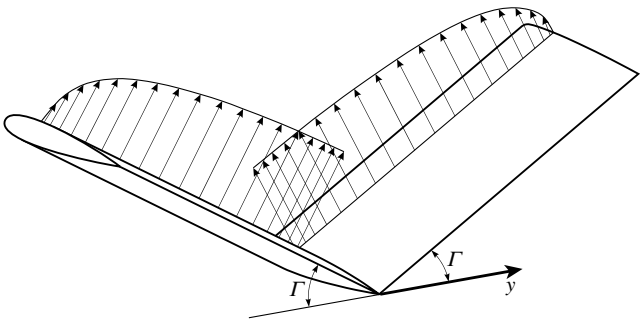

Fig. 4 Spanwise lift distribution on a V-tail at a positive angle of attack and no sideslip.

the right semispan is the normal lift multiplied by $-\sin\Gamma$. Thus, with no control surface deflection and ignoring any vortex interactions between the two semispans, the contribution that the right semispan of a V-tail makes to the vertical lift and side force could be approximated as

$$L_{\text{right}} \cong \frac{1}{2}\rho V^2 S_{\text{right}}(C_{L,\alpha})_{\Gamma=0}(\alpha_{\text{right}} + \alpha_0 - \alpha_{L0})(\cos\Gamma) \tag{3}$$

$$Y_{\text{right}} \cong \frac{1}{2}\rho V^2 S_{\text{right}}(C_{L,\alpha})_{\Gamma=0}(\alpha_{\text{right}} + \alpha_0 - \alpha_{L0})(-\sin\Gamma) \tag{4}$$

where the lift slope evaluated at $\Gamma = 0$ is simply the isolated lift slope for a horizontal stabilizer having the same semispan planform as the V-tail but with no dihedral. Similarly, the contributions from the left semispan could be approximated as

$$L_{\text{left}} \cong \frac{1}{2}\rho V^2 S_{\text{left}}(C_{L,\alpha})_{\Gamma=0}(\alpha_{\text{left}} + \alpha_0 - \alpha_{L0})(\cos\Gamma) \tag{5}$$

$$Y_{\text{left}} \cong \frac{1}{2}\rho V^2 S_{\text{left}}(C_{L,\alpha})_{\Gamma=0}(\alpha_{\text{left}} + \alpha_0 - \alpha_{L0})(\sin\Gamma) \tag{6}$$

Applying Eqs. (1) and (2) to Eqs. (3–6) and adding the contributions from the right and left semispans yields the vertical lift and side force for the complete V-tail:

$$L_{V\text{-tail}} \cong \frac{1}{2}\rho V^2 S'_V(C_{L,\alpha})_{\Gamma=0}[\alpha\cos^2\Gamma + (\alpha_0 - \alpha_{L0})\cos\Gamma] \tag{7}$$

$$Y_{V\text{-tail}} \cong -\frac{1}{2}\rho V^2 S'_V(C_{L,\alpha})_{\Gamma=0}\beta\sin^2\Gamma \tag{8}$$

where $S'_V \equiv S_{\text{right}} + S_{\text{left}}$ is the combined planform area of both semispans measured parallel with the semispan dihedral, not the horizontal projection. Using this reference area for both the lift and side-force coefficients, Eqs. (7) and (8) can be written in nondimensional form as

$$(C_L)_{V\text{-tail}} \equiv \frac{L_{V\text{-tail}}}{\frac{1}{2}\rho V^2 S'_V} \cong (C_{L,\alpha})_{\Gamma=0}[\alpha\cos^2\Gamma + (\alpha_0 - \alpha_{L0})\cos\Gamma] \tag{9}$$

$$(C_Y)_{V\text{-tail}} \equiv \frac{Y_{V\text{-tail}}}{\frac{1}{2}\rho V^2 S'_V} \cong -(C_{L,\alpha})_{\Gamma=0}\beta\sin^2\Gamma \tag{10}$$

Thus, neglecting vortex interactions between the two semispans of an isolated V-tail, the lift slope and side-force derivative are approximated as [3]

$$(C_{L,\alpha})_{V\text{-tail}} \equiv \frac{\partial}{\partial\alpha}(C_L)_{V\text{-tail}} \cong (C_{L,\alpha})_{\Gamma=0}\cos^2\Gamma \tag{11}$$

$$(C_{Y,\beta})_{V\text{-tail}} \equiv \frac{\partial}{\partial\beta}(C_Y)_{V\text{-tail}} \cong -(C_{L,\alpha})_{\Gamma=0}\sin^2\Gamma \tag{12}$$

Neglecting vortex interactions between the two semispans of a V-tail will significantly overestimate the side force. Comparison of Figs. 3 and 4 shows that a V-tail does not produce a side force in response to sideslip as efficiently as it produces a vertical force in response to an increase in angle of attack. In Fig. 3, we see that the lift generated on the two semispans of a V-tail in response to pure sideslip goes to zero at the root as well as at the tips. For this untwisted V-tail in pure sideslip to the right, the aerodynamic angle of attack relative to the freestream has a constant positive value over the right semispan and a constant negative value over the left semispan. This would tend to produce constant positive lift on the right semispan and constant negative lift on the left, if it were not for the downwash induced by the shed vorticity. The reduction in lift that occurs at the tips results in the usual manner from the tip vortices. Similarly, the reduction in lift near the root results from vorticity shed near the root.

Effect of Vortex Interactions Between the Two Semispans of a V-tail

The simplest method that can be used for closely approximating the aerodynamic derivatives associated with tail configurations similar to those shown in Figs. 1 and 2 is the numerical lifting-line method described by Phillips and Snyder [4]. For example, consider an inverted V-tail similar to that shown in the lower configuration of Fig. 1, but with no vertical stabilizer between the two semispans. Each semispan of this V-tail has a constant chord of 2.0 ft and is 6.0 ft from root to tip with a dihedral angle of −35 deg. Using an airfoil section lift slope of 2π and 50 nodes per semispan with cosine clustering, the solutions obtained at a 3.0-deg angle of attack with no sideslip and 3.0 deg sideslip with no angle of attack are shown in Fig. 5. In this figure, the vectors displayed along the quarter-chord lines show the magnitude and direction of the local section lift, and the lines along the trailing edges indicate the magnitude of the local shed vorticity per unit span. Using such numerical lifting-line computations with the reference area of 24 ft^2, the lift slope for this V-tail configuration is predicted to be $C_{L,\alpha} = 3.086$ and the change in side-force coefficient with respect to sideslip angle is found to be $C_{Y,\beta} = -1.069$.

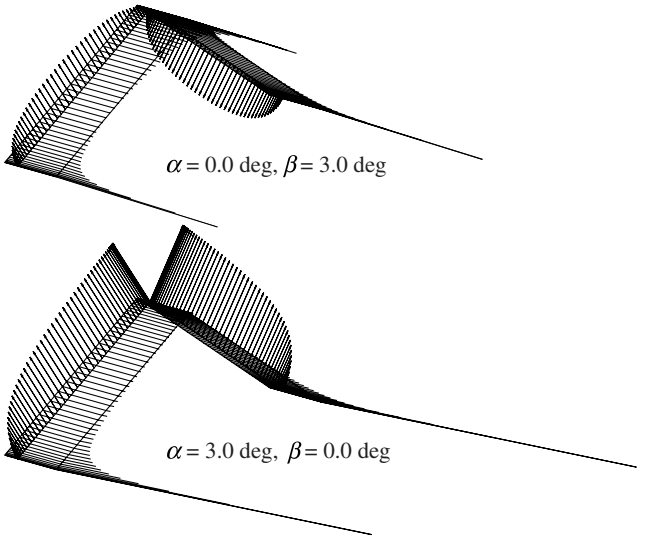

Fig. 5 Spanwise lift distributions for a V-tail, as predicted from the numerical lifting-line method.

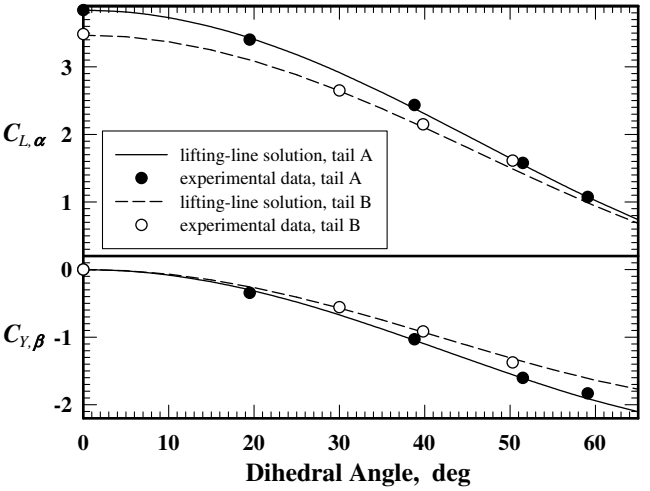

Fig. 6 Lift slope and side-force derivative as predicted from the numerical lifting-line method compared with experimental data for two V-tails with variable dihedral.

The isolated lift slope for a horizontal stabilizer having the same semispan planform as this V-tail but with no dihedral can be evaluated from the infinite series solution to Prandtl's lifting-line equation [5,6]. For this lifting surface, the aspect ratio is $R_A = 6.0$ and the taper ratio is $R_T = 1.0$. This yields $\kappa_L = 0.04$ and the lift slope is computed as

$$(C_{L,\alpha})_{\Gamma=0} = \frac{\tilde{C}_{L,a}}{(1 + \tilde{C}_{L,a}/\pi R_A)(1 + \kappa_L)} = 4.531$$

Thus, neglecting vortex interactions between the two semispans of this V-tail, the lift slope and side-force derivative from Eqs. (11) and (12) are

$$C_{L,\alpha} \cong (C_{L,\alpha})_{\Gamma=0}\cos^2\Gamma = 3.040$$

$$C_{Y,\beta} \cong -(C_{L,\alpha})_{\Gamma=0}\sin^2\Gamma = -1.491$$

Notice that for this particular V-tail, the approximate lift slope from Eq. (11) agrees with the numerical lifting-line solution to within less than 2%. However, the approximate side-force derivative determined from Eq. (12) is overestimated by nearly 40%. This is because Eq. (12) neglects the vorticity shed near the root of a V-tail in sideslip, which is shown in Fig. 5.

Although the results presented in the previous example are typical, the lift slope and side-force derivative for a V-tail depend on its planform and dihedral angle. The numerical lifting-line method is capable of closely capturing this dependence. For example, Fig. 6 shows a comparison between the results of numerical lifting-line computations and experimental data for two different V-tail planforms. The data in this figure are those presented by Purser and Campbell [3] and Schade [7]. Tail A has an aspect ratio of 5.55 and a taper ratio of 0.39, whereas tail B has an aspect ratio of 3.70 and a taper ratio of 0.56.

The dependence of the lift slope and side-force derivative on planform and dihedral for V-tails with no twist is shown in Figs. 7 and 8. Figure 7 shows the ratio of the lift slope predicted from lifting-line theory to that predicted from Eq. (11) as a function of dihedral

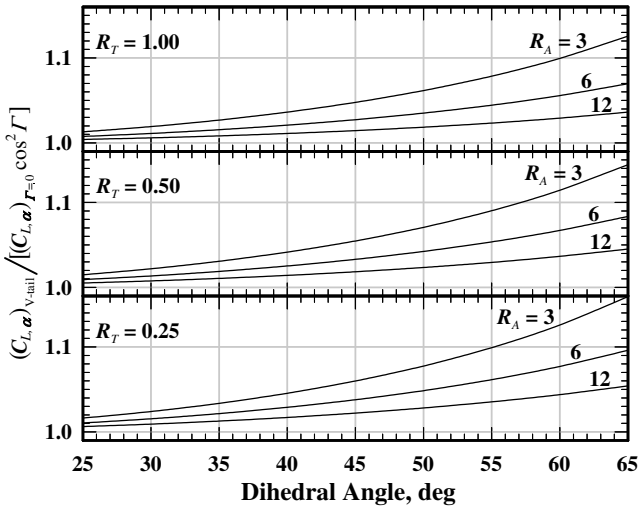

Fig. 7 Ratio of the lift slope for a V-tail as predicted from the numerical lifting-line method to that predicted from Eq. (11).

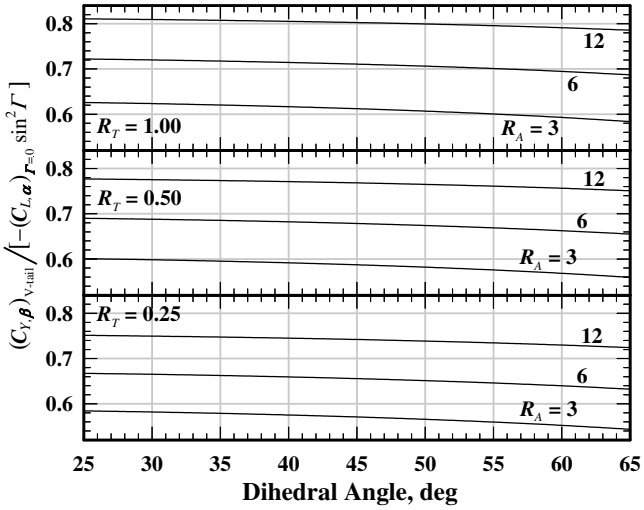

Fig. 8 Ratio of the side-force derivative for a V-tail as predicted from the numerical lifting-line method to that predicted from Eq. (12).

angle, aspect ratio, and taper ratio. Similar results for the side-force derivative are shown in Fig. 8. The V-tail aspect ratio used in these two figures is defined to be the square of twice the distance from root to tip, divided by the total area of both semispans combined (not the horizontal projection). Although these figures were generated for upright V-tails with positive dihedral, they may also be applied to inverted V-tails with anhedral.

In the preliminary design of an aircraft, we may wish to study some of the tradeoffs between using a conventional tail or a V-tail. Such trade studies require a comparison between two tail configurations that provide the same level of static stability for both pitch and yaw. Figures 7 and 8 can be used to aid in making an initial estimate for the V-tail geometry that will provide the required stability.

Use of Horizontal-Stabilizer Dihedral in Combination with a Vertical Stabilizer

Although an aft V-tail with no vertical stabilizer can be used to provide both pitch and yaw stability for an airplane, the aerodynamic interactions between the two semispans of a V-tail reduce its effectiveness in producing a side force in response to sideslip. When a V-tail is used in combination with a vertical stabilizer, as shown in Fig. 1, the aerodynamic interactions between the three lifting surfaces of the tail become more complex and sometimes produce results that are unexpected.

To give the reader insight into the performance of tail configurations like those shown in Fig. 1, we start by examining the lift distribution on a conventional tail. Figure 9 shows a typical lift distribution for a conventional tail in pure sideslip, as predicted from numerical lifting-line computations. For those who might wish to duplicate these computations, this particular tail has a horizontal aspect ratio of 4.0 and a horizontal planform area of 36 ft^2. The vertical stabilizer has the same constant chord with a planform area of 12 ft^2. In this example, both the horizontal and vertical surfaces have thin symmetric airfoil sections and no twist. The sweep for both surfaces is zero and the horizontal surface has no dihedral. At zero angle of attack, lifting-line computations for this geometry predict a change in side-force coefficient with respect to sideslip angle of −3.078, based on the vertical reference area. The aerodynamic section forces shown in Fig. 9 were computed at zero angle of attack. All of the forces that are shown in this figure result from a 5-deg sideslip angle.

The lift shown on the vertical stabilizer in Fig. 9 goes to zero at the upper tip as a result of the wingtip vortex shed in this vicinity. If the vertical stabilizer were isolated in the freestream without the horizontal stabilizer, the lift would also go to zero at the lower extremity, and a strong wingtip vortex would be shed in this region as well. However, the horizontal stabilizer acts like large winglets at the base of the vertical stabilizer and inhibits vortex shedding in this vicinity. The vorticity generated on the vertical stabilizer is spread out over both sides of the horizontal stabilizer. This prevents the lift on the vertical stabilizer from going to zero at the root and generates additional lift on the horizontal stabilizer. The lift developed on the left semispan of the horizontal stabilizer is upward, whereas that on the right semispan is downward. All aerodynamic forces shown on this horizontal stabilizer result from vortex interactions with the vertical stabilizer.

Another way to look at the origin of the forces acting on this horizontal stabilizer at zero aerodynamic angle of attack is to realize that low pressure generated on the left side of the vertical stabilizer creates positive lift on the left side of the horizontal stabilizer. Similarly, the high pressure to the right of the vertical stabilizer will generate negative lift on the right semispan of the horizontal stabilizer.

When a small amount of positive dihedral is added to the horizontal stabilizer of a conventional tail, the lift distribution shown in Fig. 9 is changed in two important ways. First and perhaps most obvious, positive dihedral in the horizontal stabilizer combined with sideslip to the right adds positive lift to the right semispan and negative lift to the left semispan, similar to that shown on the V-tail in Fig. 3. With the added positive dihedral, this change tends to increase the side force to the left. The second change to the lift distribution shown in Fig. 9, which arises from adding positive dihedral to the horizontal stabilizer, is simply a tilting of the lift vectors that are shown on the horizontal stabilizer in this figure. The positive lift vectors on the left semispan are tilted to the right and the negative lift vectors on the right semispan are also tilted to the right. This change tends to decrease the side force to the left. Figure 10 shows the net effect of these two changes when 10 deg of dihedral are added to the horizontal stabilizer of the conventional tail shown in Fig. 9. Notice that the lift vectors near the root of the horizontal stabilizer in Fig. 10

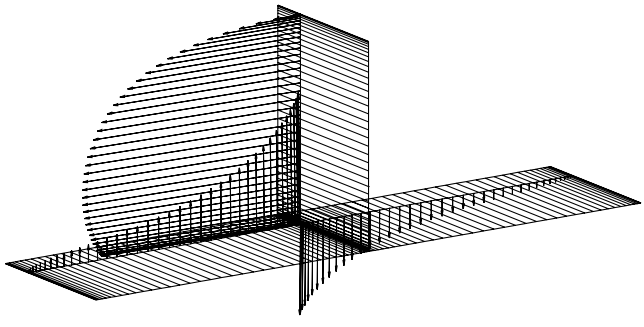

Fig. 9 Lift distribution on a conventional tail in pure sideslip.

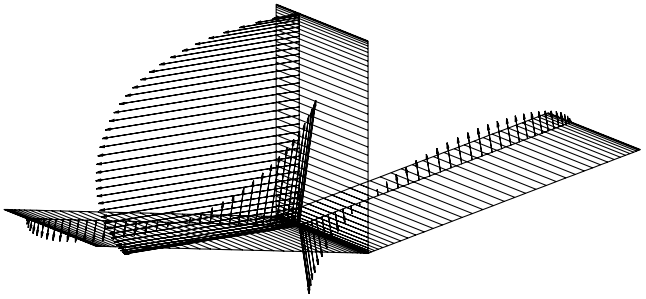

Fig. 10 Effect of horizontal-stabilizer dihedral on the lift distribution for a conventional tail in pure sideslip.

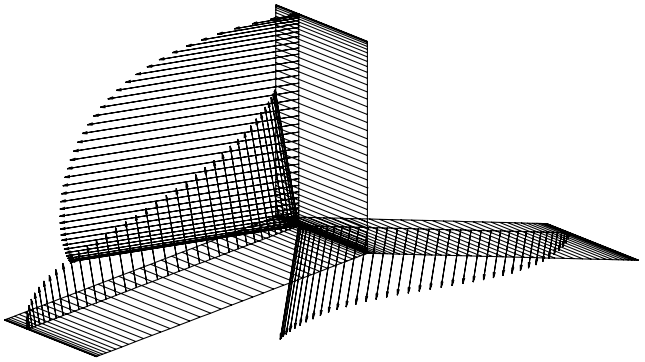

Fig. 11 Effect of horizontal-stabilizer anhedral on the lift distribution for a conventional tail in pure sideslip.

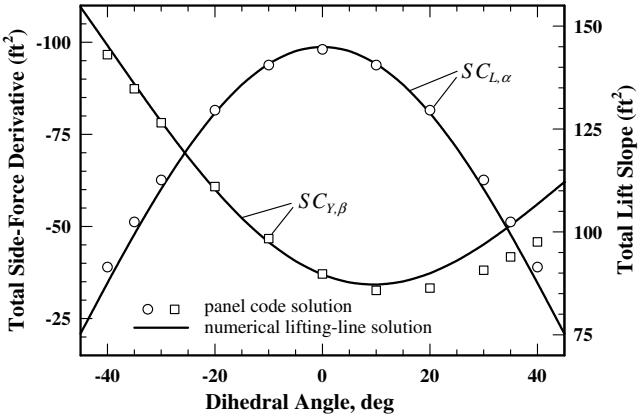

Fig. 12 Effect of horizontal-stabilizer dihedral on the side-force derivative and lift slope, for the conventional tail shown in Fig. 9.

contribute to a decrease in the side force to the left, whereas the lift vectors on the outboard sections contribute to an increase in the side force to the left. For this example, the net effect of adding 10 deg of dihedral to the horizontal stabilizer is a 7% reduction in the total magnitude of the side force, in spite of a 52% increase in the vertical projection of the total planform area.

Figure 11 shows the effect of adding 10 deg of anhedral to the horizontal stabilizer of the conventional tail shown in Fig. 9. In this case, the lift generated on the horizontal stabilizer as a result of vortex interactions with the vertical stabilizer is in the same direction as the lift generated by the direct effects of the horizontal-stabilizer anhedral. Thus, both effects contribute to increasing the side force to the left. For this particular example, the net effect of the 10-deg anhedral is a 24% increase in the magnitude of the side force.

Figure 12 shows how the side-force derivative for the conventional tail shown in Fig. 9 varies with the horizontal-stabilizer dihedral angle. The solid lines plotted in this figure were obtained from numerical lifting-line computations by varying only the dihedral angle of the horizontal stabilizer while keeping its chord and total planform area constant. For comparison, the square and circular markers display results obtained for the same geometry using a numerical panel code. The results are plotted in terms of what is being called the *total side-force derivative* in square feet. This is simply the product of the change in side-force coefficient with respect to sideslip angle and the corresponding reference area. This total side-force derivative is also equal to the change in total side force with respect to sideslip angle divided by the dynamic pressure. Similar results for the change in lift with respect to angle of attack are also shown in Fig. 12.

From the results shown in Fig. 12, we see that adding a small amount of anhedral to the horizontal stabilizer of a conventional tail produces a significant increase in its ability to provide static yaw stability for an airplane, while only slightly reducing its ability to provide static pitch stability. On the other hand, adding the same amount of positive dihedral to the horizontal stabilizer of the same conventional tail will actually reduce the tail's effectiveness in providing both pitch and yaw stability.

The results plotted in Fig. 12 also show that when larger dihedral angles are used in tail configurations like those shown in Fig. 1, the tail will provide greater yaw stability when the dihedral in the horizontal stabilizer has the opposite sign from that of the vertical stabilizer. For example, with the geometry used for Fig. 12, the configuration with 35 deg of anhedral provides over 75% more yaw stability than a similar configuration with 35 deg of positive dihedral. The reason for the difference can be seen by comparing the two lift distributions for pure sideslip, which are shown in Fig. 13.

Although the lift distributions shown in Fig. 13 were obtained using the vortex theory of lift, the lifting forces are transmitted to the surfaces through pressure variations in the air flowing over the tail. The generalized vortex lifting law [8], which makes three-dimensional lifting-line computations possible, greatly simplifies the mathematical description of lift. However, it can be difficult to visualize the origin of lift distributions, such as those shown in

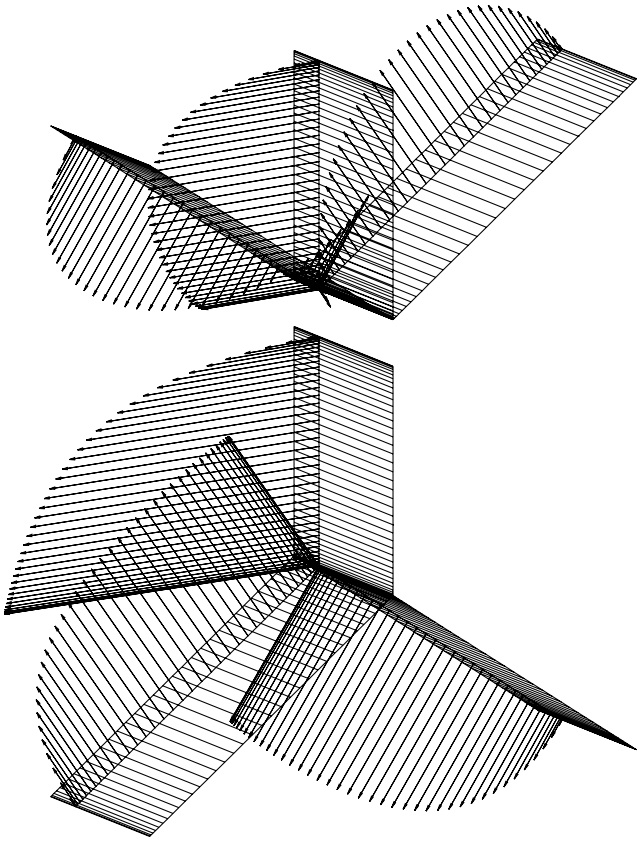

Fig. 13 Lift distributions on two similar tail configurations with opposite dihedral.

Fig. 13, directly from vortex theory. Another way to look at such lift distributions is through our knowledge of the pressure distributions about lifting surfaces.

Consider, for example, the three lifting surfaces shown in the upper configuration of Fig. 13. If each of these lifting surfaces were isolated in a freestream and subjected to positive sideslip, high pressure would develop to the right of the surface and low pressure would develop on the left in all three cases. However, when these three surfaces are combined in the freestream and subjected to positive sideslip, there will be some conflicting forces at work in the region where the surfaces are joined. In the triangular region to the left of the vertical surface and to the right of the left-hand surface, the vertical surface is attempting to produce low pressure while the left-hand surface is attempting to produce high pressure. Near the root where the two surfaces are in close proximity, the vertical surface will prevail in this competition, because its orientation relative to the sideslip velocity component produces a greater freestream angle of attack on the surface. Thus, low pressure in the region immediately above and to the left of the root of the vertical stabilizer contributes to a leftward force on the vertical surface and a rightward force on the left-hand surface, as shown in Fig. 13. In a similar manner, high pressure in the region just above and to the right of the root of the vertical stabilizer will contribute to a leftward force on the vertical surface and a rightward force on the right-hand surface. By similar reasoning, complementary pressure distributions can be used to justify the more favorable lift distribution that is shown on the lower configuration of Fig. 13.

Reducing Tail Size with Horizontal-Stabilizer Dihedral

The results shown in Fig. 12 suggest that the weight and parasitic drag for a conventional tail could be reduced somewhat, without sacrificing pitch or yaw stability, by adding anhedral and area to the horizontal stabilizer while decreasing the area of the vertical stabilizer. For the conventional tail geometry shown in Fig. 9, the results plotted in Fig. 14 show how the area of the horizontal and vertical stabilizers can be varied with horizontal-stabilizer dihedral angle to maintain constant pitch and yaw stability. The data plotted in this figure were obtained from numerical lifting-line computations. For each dihedral angle, the chord was held constant and the root-to-tip lengths for the horizontal and vertical stabilizers were adjusted iteratively, using Newton's method, to maintain the same total lift slope and side-force derivative as the original conventional tail with no dihedral. As either positive or negative dihedral is added to this conventional tail, the area of the horizontal stabilizer is increased to maintain constant total lift slope. When negative dihedral is added to the horizontal stabilizer, the area of the vertical stabilizer can be reduced, because a portion of the required side force is supported by the horizontal stabilizer. Thus, as anhedral is added to the horizontal stabilizer, its area increases but the area of the vertical stabilizer can be decreased. When the anhedral in the horizontal stabilizer becomes large enough, the required vertical-stabilizer area goes to zero, which yields a V-tail with the same total lift slope and side-force derivative as the original conventional tail.

With all other things being equal, tail weight and parasitic drag are approximately proportional to the total area of the horizontal and vertical stabilizers combined. This total combined area is also plotted in Fig. 14. Notice that for the conventional tail geometry shown in Fig. 9, the total required area continues to decrease as anhedral is added to the horizontal stabilizers, until the vertical-stabilizer area goes to zero. Thus, a V-tail provides the minimum-area solution in this particular case and results in a total area reduction of more than 5%, relative to the base conventional tail with no horizontal-stabilizer dihedral. This is typical for applications where the required vertical planform is significantly less than the required horizontal planform. In this particular case, the vertical planform of the base conventional tail is only one-third of the horizontal planform.

When the ratio of the required vertical planform to the required horizontal planform is larger, a V-tail may not provide the minimum-area solution. For example, Fig. 15 shows results similar to those

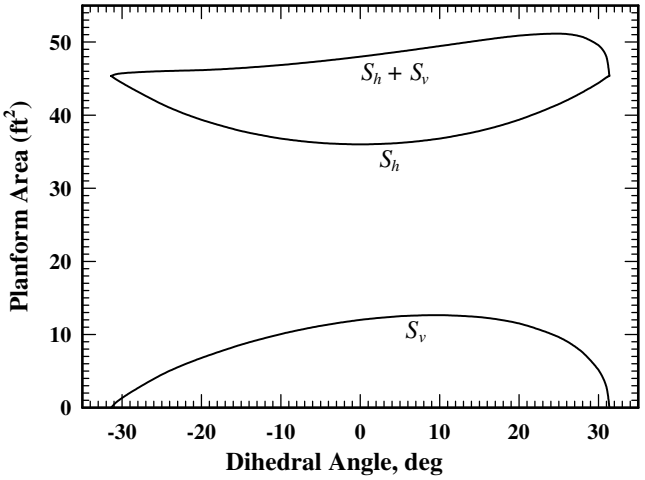

Fig. 14 Effect of horizontal-stabilizer dihedral on the tail area required to maintain the same total lift slope and side-force derivative as the conventional tail shown in Fig. 9.

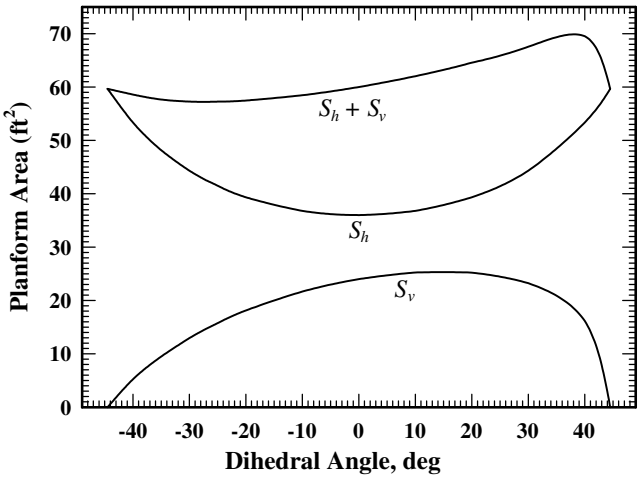

Fig. 15 Effect of horizontal-stabilizer dihedral on the tail area required to maintain constant total lift slope and side-force derivative for a tail with larger vertical planform requirements.

plotted in Fig. 14, but for a tail geometry having a base vertical-stabilizer area that is two-thirds of that for the horizontal stabilizer. The base conventional tail used for this figure has a horizontal aspect ratio of 4.0 and a horizontal planform area of 36 ft^2. The vertical stabilizer has the same root chord with a planform area of 24 ft^2. Both the horizontal and vertical surfaces have taper ratios of 0.5, thin symmetric airfoil sections, and no twist. The quarter-chord sweep for both surfaces is zero and the horizontal surface has no dihedral. At zero angle of attack, lifting-line computations for this geometry predict a total side-force derivative $SC_{Y,\beta}$ of -96.68 ft^2 and a total lift slope $SC_{L,\alpha}$ of 148.90 ft^2.

For this base tail geometry, lifting-line computations predict a minimum-area solution at a horizontal-stabilizer dihedral angle of approximately -27 deg with a vertical-stabilizer area of just over 14.7 ft^2. This minimum-area solution has a total area of about 57.2 ft^2, which is nearly 5% less than the total area of the base conventional tail and more than 4% less than that required for an equivalent V-tail. Figure 15 also shows that adding positive dihedral to this base conventional tail can increase the total required area by as much as 15%.

Effects of Tail Dihedral on Static Roll Stability

When dihedral is used in the horizontal stabilizer of an aft tail, it influences static roll stability in much the same way as dihedral in the

main wing does. For example, when a V-tail like that shown in Fig. 2 is subjected to sideslip, it produces a significant rolling moment as well as a side force. This can be seen in Fig. 3.

Dihedral affects the roll stability derivative because it causes the lift on the right and left semispans to respond differently to sideslip. From Eqs. (1) and (2), a small amount of sideslip produces a change in angle of attack that can be closely approximated for the right and left semispans of a V-tail as

$$(\Delta\alpha)_{\text{right}} = \beta \sin\Gamma \tag{13}$$

$$(\Delta\alpha)_{\text{left}} = -\beta \sin\Gamma \tag{14}$$

The differential in angle of attack between the right and left semispans creates a differential in lift that produces a rolling moment. From Fig. 4, we see that positive lift on the left semispan ($y < 0$) produces a positive rolling moment, whereas positive lift on the right semispan ($y > 0$) produces a negative rolling moment. Thus, the rolling moment arm about the junction of the two semispans for the lift developed on any section of the V-tail is $-y/\cos\Gamma$ and the differential length measured perpendicular to the airfoil sections of the V-tail is $dy/\cos\Gamma$. Using the approximation for small sideslip angles given by Eqs. (13) and (14), the net rolling moment coefficient that results from sideslip combined with V-tail dihedral can be written [9]

$$\begin{aligned}(C_\ell)_{V\text{-tail}} &= \int_{y=-b_V/2}^{0} \frac{\tilde{C}_{L_i,\alpha} c}{Sb}(-\beta\sin\Gamma)\frac{-y}{\cos\Gamma}\frac{dy}{\cos\Gamma} \\ &\quad + \int_{y=0}^{b_V/2} \frac{\tilde{C}_{L_i,\alpha} c}{Sb}(\beta\sin\Gamma)\frac{-y}{\cos\Gamma}\frac{dy}{\cos\Gamma} \\ &= -\frac{\beta\sin\Gamma}{Sb\cos^2\Gamma}\int_{y=-b_V/2}^{b_V/2} \tilde{C}_{L_i,\alpha} c|y|dy\end{aligned} \tag{15}$$

The spanwise variation of local induced downwash is affected by the sideslip. Thus, the derivative of Eq. (15) with respect to β must be written as

$$\begin{aligned}\frac{\partial}{\partial\beta}(C_\ell)_{V\text{-tail}} &= -\frac{\sin\Gamma}{Sb\cos^2\Gamma} \\ &\quad \times \left(\int_{y=-b_V/2}^{b_V/2} \tilde{C}_{L_i,\alpha} c|y|dy + \beta\int_{y=-b_V/2}^{b_V/2} \frac{\partial\tilde{C}_{L_i,\alpha}}{\partial\beta} c|y|dy\right)\end{aligned}$$

However, the roll stability derivative is evaluated at $\beta = 0$ and the contribution of the V-tail to this aerodynamic derivative can be written

$$(C_{\ell,\beta})_{V\text{-tail}} = -\frac{\sin\Gamma}{Sb\cos^2\Gamma}\left[\int_{y=-b_V/2}^{b_V/2} \tilde{C}_{L_i,\alpha} c|y|dy\right]_{\beta=0} \tag{16}$$

Because the integral in Eq. (16) is evaluated at $\beta = 0$, both the flow and geometry are symmetric about the midspan. Thus, the integration from $-b_V/2$ to 0 is equivalent to that from 0 to $b_V/2$, and Eq. (16) can also be written as

$$\begin{aligned}(C_{\ell,\beta})_{V\text{-tail}} &= -\frac{2\sin\Gamma}{Sb\cos^2\Gamma}\left[\int_{y=0}^{b_V/2} \tilde{C}_{L_i,\alpha} c y dy\right]_{\beta=0} \\ &= -\frac{2\sin\Gamma}{Sb}\left[\int_{y'=0}^{b'_V/2} \tilde{C}_{L_i,\alpha} c y' dy'\right]_{\beta=0}\end{aligned} \tag{17}$$

where $y' \equiv y/\cos\Gamma$ is a spanwise coordinate measured parallel with the tail dihedral and $b'_V \equiv b_V/\cos\Gamma$ is twice the root-to-tip semispan length.

For low Mach number, Prandtl's lifting-line theory can be used to determine the spanwise variation of an in situ section lift slope, which is needed to evaluate the integral on the right-hand side of Eq. (17). In general, it is necessary to use a numerical lifting-line solution, because the classical infinite series solution applies only to lifting surfaces with no dihedral. However, we shall begin by neglecting the spanwise variation of the in situ section lift slope caused by the V-tail dihedral. The integral in Eq. (17) can then be evaluated from the classical solution to Prandtl's lifting-line equation. For an unswept lifting surface of arbitrary planform and twist, this solution predicts that the change in local section lift coefficient with respect to the semispan angle of attack is given by [9]

$$\tilde{C}_{L_i,\alpha} = \frac{4b'_V}{c}\sum_{n=1}^{\infty} a_n \sin(n\theta) \tag{18}$$

where a_n denotes the planform coefficients in the infinite series solution to the lifting-line equation [5,6] and θ is defined by the change of variables

$$y' \equiv \frac{1}{2}b'_V\cos\theta \tag{19}$$

$$dy' = -\frac{1}{2}b'_V\sin\theta d\theta \tag{20}$$

Using Eqs. (18–20) in Eq. (17) results in

$$\begin{aligned}(C_{\ell,\beta})_{V\text{-tail}} \cong -\frac{2\sin\Gamma}{Sb}\int_{\theta=\pi/2}^{0}&\left(\frac{4b'_V}{c}\sum_{n=1}^{\infty} a_n\sin(n\theta)\right) \\ &\times c\left(\frac{1}{2}b'_V\cos\theta\right)\left(-\frac{1}{2}b'_V\sin\theta d\theta\right)\end{aligned}$$

After using the trigonometric identity $\sin(2\theta) = 2\sin\theta\cos\theta$, this reduces to

$$(C_{\ell,\beta})_{V\text{-tail}} \cong -\frac{b'^3_V\sin\Gamma}{Sb}\sum_{n=1}^{\infty} a_n\int_{\theta=0}^{\pi/2}\sin(n\theta)\sin(2\theta)d\theta \tag{21}$$

The integral on the right-hand side of Eq. (21) is readily evaluated to yield

$$\int_{\theta=0}^{\pi/2}\sin(n\theta)\sin(2\theta)d\theta = \begin{cases} 2\sin(n\pi/2)/(4-n^2), & n \neq 2 \\ \pi/4, & n = 2\end{cases}$$

Using this result in Eq. (21) gives

$$(C_{\ell,\beta})_{V\text{-tail}} \cong -\frac{b'^3_V}{Sb}\left[\frac{2}{3}a_1 + \frac{\pi}{4}a_2 + \sum_{n=3}^{\infty}\frac{2\sin(n\pi/2)}{4-n^2}a_n\right]\sin\Gamma \tag{22}$$

From the classical lifting-line solution, the isolated lift slope for a horizontal stabilizer having the same semispan planform as the V-tail but with no dihedral is given by [5,6]

$$(C_{L,\alpha})_{\Gamma=0} = \pi(b'^2_V/S'_V)a_1$$

Thus, Eq. (22) can be rearranged as

$$(C_{\ell,\beta})_{V\text{-tail}} \cong -\frac{2S'_V b'_V}{3\pi Sb}\kappa_\ell(C_{L,\alpha})_{\Gamma=0}\sin\Gamma \tag{23}$$

The planform factor for roll stability was presented by Phillips [9]:

$$\kappa_\ell = 1 + \frac{3\pi}{8}\frac{a_2}{a_1} + \sum_{n=3}^{\infty}\frac{3\sin(n\pi/2)}{4-n^2}\frac{a_n}{a_1} \tag{24}$$

Because the series solution to Prandtl's lifting-line equation applies to unswept lifting surfaces with any spanwise variation in section geometry, Eq. (24) can be used for an unswept V-tail of any planform with arbitrary geometric and aerodynamic twist [10–12].

Like Eqs. (11) and (12), the approximation given by Eq. (23) neglects the vortex interactions between the two semispans of the isolated V-tail. Although the vortex interactions between the different lifting surfaces of the tail are commonly neglected in the early phases of aircraft design, this practice will significantly

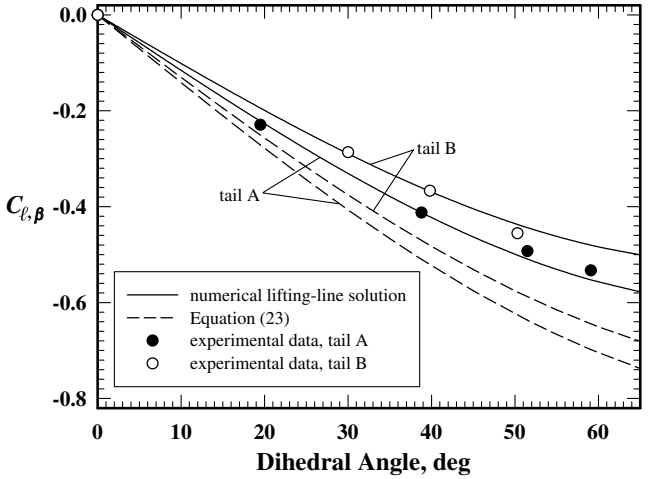

Fig. 16 The roll stability derivative as predicted from numerical lifting-line computations and Eq. (23), compared with experimental data for two V-tails with variable dihedral.

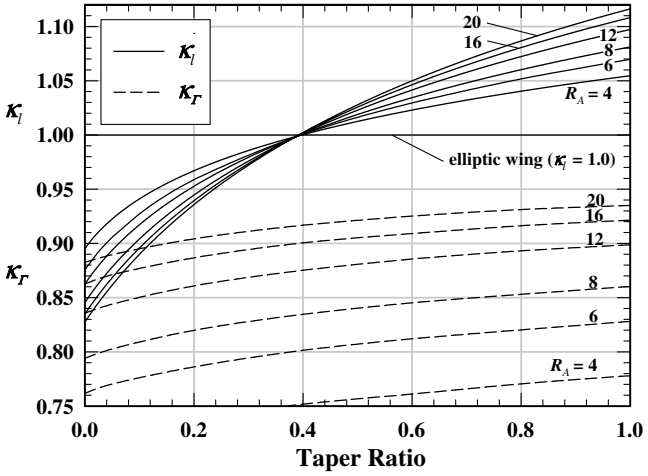

Fig. 17 The small-angle dihedral factors for lifting surfaces with linear taper.

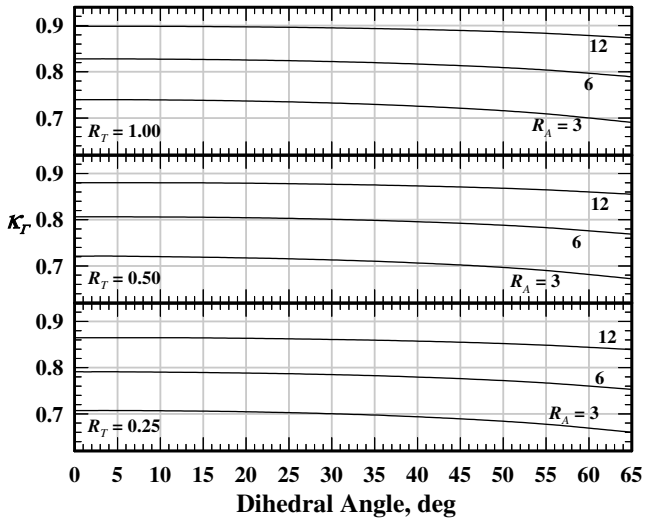

Fig. 18 The dihedral factor for the vortex interactions between the semispans of a V-tail.

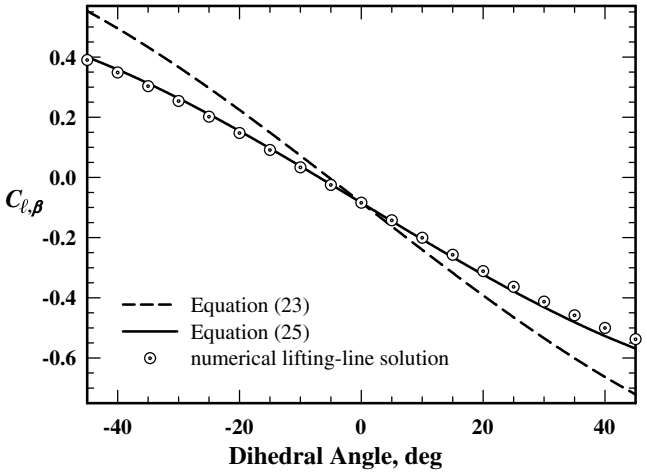

Fig. 19 Effect of horizontal-stabilizer dihedral on the roll stability derivative, for the tail geometry that was used in Figs. 9–13.

overestimate the roll stability contribution of a V-tail. For example, Fig. 16 shows a comparison between the results of numerical lifting-line computations, Eq. (23), and experimental data for two different V-tail planforms. The data in this figure are those presented by Purser and Campbell [3] and Schade [7]. Tail A has an aspect ratio of 5.55 and a taper ratio of 0.39, whereas tail B has an aspect ratio of 3.70 and a taper ratio of 0.56. The results presented in Fig. 16 show that, while numerical lifting-line computations will closely predict the roll stability contribution of a V-tail, neglecting vortex interactions between the two semispans overestimates this contribution by 25 to 35%.

An additional correction factor can be applied to Eq. (23) to account for the vortex interactions between the two semispans of an isolated V-tail,

$$(C_{\ell,\beta})_{V\text{-tail}} = -\frac{2S'_V b'_V}{3\pi Sb}\kappa_\Gamma \kappa_\ell (C_{L,\alpha})_{\Gamma=0} \sin\Gamma \tag{25}$$

For small dihedral angles, κ_Γ is independent of Γ. For lifting surfaces with linear taper, Fig. 17 shows how κ_ℓ and the small-angle value for κ_Γ vary with aspect ratio and taper ratio as predicted from lifting-line computations. A reasonable first-order correction to Eq. (23) is obtained by using Eq. (25) with the small-angle value for κ_Γ, which can be evaluated from Fig. 17. However, the results plotted in Fig. 17 strictly apply only for small dihedral angles. For the larger dihedral angles commonly used in a V-tail, κ_Γ depends somewhat on the tail dihedral as well as the semispan planform. For lifting surfaces with linear taper, Fig. 18 shows how κ_Γ varies with dihedral angle, aspect ratio, and taper ratio, as predicted from numerical lifting-line computations.

When horizontal-stabilizer dihedral is used in combination with a vertical stabilizer as shown in Fig. 1, Eq. (25) can be used to estimate the roll stability contribution resulting from the horizontal-stabilizer dihedral. The contribution predicted from Eq. (25) must be added to that for a tail having the same lifting-surface geometry but with no horizontal-stabilizer dihedral. Figure 19 shows how the roll stability derivative for the tail geometry used in Figs. 9–13 varies with horizontal-stabilizer dihedral angle. The solid line plotted in this figure was obtained by adding results from Eq. (25) to the roll stability derivative for the conventional tail with no horizontal-stabilizer dihedral. The dashed line shows results obtained similarly from Eq. (23). For comparison, the circular markers display results obtained for the actual tail geometry using numerical lifting-line computations.

Conclusions

Horizontal-stabilizer dihedral can significantly influence the static stability of an airplane. The vortex interactions between the lifting surfaces of an aft tail substantially alter the side force developed on

the tail as a result of sideslip. In the case of a V-tail, these vortex interactions depend on the dihedral angle and semispan planform. The numerical lifting-line method is shown to be capable of closely capturing this dependence. Such computations show that vortex interactions between the two semispans of a V-tail slightly increase the change in lift with respect to angle of attack and substantially decrease the change in side force and rolling moment with respect to sideslip angle. Nevertheless, for applications where the required vertical planform is significantly less than the required horizontal planform, using a V-tail in place of a conventional tail with no horizontal-stabilizer dihedral has the potential for reducing tail weight by about 5%, based on required area alone. On the other hand, the control mechanism for a V-tail is more complex than that for a conventional tail and this added complexity could add more weight than is saved by the reduction in tail area. Another advantage commonly given for the V-tail is a reduction in interference drag due to the fact that a V-tail requires only two fuselage-tail junctions rather than three, which are required for a conventional tail.

When horizontal-stabilizer dihedral is used in combination with a vertical stabilizer as shown in Fig. 1, the tail will provide greater yaw stability when the dihedral in the horizontal stabilizer has the opposite sign from that of the vertical stabilizer. Specifically, a conventional tail having an upright vertical stabilizer mounted above a horizontal stabilizer works best when anhedral is used in the horizontal stabilizer. Conversely, an inverted vertical stabilizer with -90 deg dihedral, or a traditional T-tail, works best when positive dihedral is used in the horizontal stabilizer. If the ratio of the required vertical planform to the required horizontal planform is large enough, properly utilizing horizontal-stabilizer dihedral can result in a minimum tail weight that is less than that for either a V-tail or a conventional tail with no horizontal-stabilizer dihedral.

Although adding positive dihedral to the horizontal stabilizer of a conventional tail will increase the roll stability of an airplane, this is not a particularly efficient way to provide roll stability. There are two primary reasons for this. First, because the span of the horizontal stabilizer is typically much less than that for the wing, the moment arm available for generating a rolling moment on the horizontal stabilizer is small. In addition, a small amount of positive dihedral in the horizontal stabilizer of a conventional tail will significantly decrease the yaw stability provided by the tail. On the other hand, adding positive dihedral to the horizontal stabilizer of a T-tail increases both roll and yaw stability for the airplane.

References

[1] Kidd, J. A., "Investigation of the Effect of Variable Tail Dihedral on Airplane Stability and Control," AIAA Paper 1988-4335, Aug. 1988.

[2] Abzug, M. J., "V-Tail Stalling at Combined Angles of Attack and Sideslip," *Journal of Aircraft*, Vol. 36, No. 4, 1999, pp. 729–731.

[3] Purser, P. E., and Campbell, J. P., "Experimental Verification of a Simplified Vee-Tail Theory and Analysis of Available Data on Complete Models with Vee Tails," NACA TR-823, 1945.

[4] Phillips, W. F., and Snyder, D. O., "Modern Adaptation of Prandtl's Classic Lifting-Line Theory," *Journal of Aircraft*, Vol. 37, No. 4, 2000, pp. 662–670.

[5] Katz, J., and Plotkin, A., "Finite Wing: The Lifting-Line Model," *Low-Speed Aerodynamics*, 2nd ed., Cambridge Univ. Press, Cambridge, 2001, pp. 167–183.

[6] Phillips, W. F., "Prandtl's Classical Lifting-Line Theory," *Mechanics of Flight*, Wiley, Hoboken, NJ, 2004, pp. 45–53.

[7] Schade, R. O., "Effects of Geometric Dihedral on the Aerodynamic Characteristics of Two Isolated Vee-Tail Surfaces," NACA TN-1369, July 1947.

[8] Saffman, P. G., "Vortex Force and Bound Vorticity," *Vortex Dynamics*, Cambridge Univ. Press, Cambridge, 1992, pp. 46–48.

[9] Phillips, W. F., "Analytical Solution for Wing Dihedral Effect," *Journal of Aircraft*, Vol. 39, No. 3, 2002, pp. 514–516.

[10] Phillips, W. F., "Lifting-Line Analysis for Twisted Wings and Washout-Optimized Wings," *Journal of Aircraft*, Vol. 41, No. 1, 2004, pp. 128–136.

[11] Phillips, W. F., Alley, N. R., and Goodrich, W. D., "Lifting-Line Analysis of Roll Control and Variable Twist," *Journal of Aircraft*, Vol. 41, No. 5, 2004, pp. 1169–1176.

[12] Phillips, W. F., Fugal, S. R., and Spall, R. E., "Minimizing Induced Drag with Wing Twist, Computational-Fluid-Dynamics Validation," *Journal of Aircraft*, Vol. 43, No. 2, 2006, pp. 437–444.